Int. J. Heat Mass Transfer. Vol. 19, pp. 41–49. Pergamon Press 1976. Printed in Great Britain

TRANSFER CHARACTERISTICS OF TWO-ROW PLATE FIN AND TUBE HEAT EXCHANGER CONFIGURATIONS

F. E. M. SABOYA and E. M. SPARROW
Department of Mechanical Engineering, University of Minnesota, Minneapolis, MN 55455, U.S.A.

(*Received* 6 *September* 1974 *and in revised form* 17 *January* 1975)

Abstract—The heat-mass transfer analogy, in conjunction with the naphthalene sublimation technique, was used to investigate the transfer capabilities and transfer mechanisms in two-row plate fin and tube heat exchanger configurations. Local and average transfer coefficients were determined from measurements of the mass transferred in an analogical system consisting of a pair of naphthalene plates and an array of spacer disks. The analogical system modeled a typical heat exchanger flow passage. The results were presented in dimensionless form to facilitate their conversion to Nusselt numbers.

Different transfer mechanisms were found to be operative on the portions of the fin which are respectively associated with the first and the second rows of tubes. For the portion associated with the first row, the two factors which provided high mass-transfer rates were the boundary layer on the forward part of the fin and a vortex system which develops in front of the tubes. On the other hand, for the portion of the fin associated with the second row, there is no boundary-layer regime, and it is the vortex system alone which is responsible for high transfer rates. At higher Reynolds numbers, the influence of the second-row vortex system is sufficient to cause a near equality in the transfer capabilities of the first-row and second-row fin surfaces.

NOMENCLATURE

- D, tube diameter;
- D_h, hydraulic diameter, equation (5);
- $\mathscr{D}$, diffusion coefficient;
- h, spacing between plates;
- K, local mass-transfer coefficient, equation (4);
- $\bar{K}$, average mass-transfer coefficient, equation (6);
- L, streamwise length of channel;
- $\dot{m}$, local rate of mass transfer/area;
- $\dot{M}$, surface-integrated mass-transfer rate;
- $\dot{M}_{\mathrm{I}}$, $\dot{M}_{\mathrm{II}}$, surface-integrated mass-transfer rates for regions I and II;
- $\dot{M}'$, spanwise-integrated mass-transfer rate;
- Pr, Prandtl number;
- Re, Reynolds number, equation (9);
- S, distance between tube centers;
- Sc, Schmidt number;
- Sh, local Sherwood number, equation (4);
- $\overline{Sh}$, average Sherwood number, equation (6);
- x, y, surface coordinates, Fig. 1.

Greek symbols

- δ, local sublimation depth;
- ν, kinematic viscosity;
- $\rho_{n,b}$, bulk concentration of naphthalene vapor;
- $\rho_{n,w}$, wall concentration of naphthalene vapor.

INTRODUCTION

PLATE fin and tube heat exchangers are employed in a wide variety of engineering applications, for instance, in air conditioning machines, process gas heaters and coolers, compressor intercoolers and aftercoolers, etc. Depending on the application, there may be one or more rows of tubes situated in the flow channels formed by the array of parallel plate fins. These various heat exchangers are frequently designated as one-row coils, two-row coils, etc. A recent survey by Rich [1] of published heat-transfer information relating to such heat exchange devices revealed a surprising sparsity. Whatever heat-transfer information is available is in the form of average transfer coefficients.

Very recently, it was demonstrated [2] that the analogy between heat and mass transfer is a viable approach not only for obtaining overall transfer coefficients, but also for obtaining local transfer coefficients on the fin surfaces. The mass-transfer experiments were performed utilizing the naphthalene sublimation technique.

In [2], the analogy method was employed to investigate the transfer characteristics of one-row coils. The local measurements revealed high values of the transfer coefficients on the forward part of the fin due to the presence of developing boundary layers. In addition, owing to a natural augmentation effect caused by a vortex system which develops in front of the tube, high transfer coefficients were found to exist in a U-shaped band that rings the tube. The effect of the vortex system was more pronounced at higher Reynolds numbers. Relatively low transfer coefficients were encountered on that part of the fin that lies downstream of the minimum flow cross section, with particularly low values in the wake behind the tube.

If consideration is given to two-row coils, it might be expected that the transfer mechanisms associated with the second row of the coil would be different from those just discussed for the first row (i.e. those for a one-row coil). First of all, boundary-layer development, which causes high transfer rates on the forward part of the fin upstream of the first row of tubes, is an irrelevant consideration for the portion of the fin associated with the second row. The developing

boundary layers have long since coalesced before the flow reaches the vicinity of the second row. Second, the wake shed from the tubes of the first row will wash the downstream portions of the fin, thereby affecting the fin transfer coefficients of the second row. Also, at the higher Reynolds numbers, the vortex system generated in front of the tubes of the first row is swept downstream and should, therefore, influence the second-row transfer coefficients. Finally, whereas the same fluid flow phenomena that are responsible for the vortex system in front of the first row should also be operative for the second row, they now must operate in a much more disturbed flow field.

Quantitative information on the transfer characteristics of two-row plate fin and tube heat exchangers appears to be unavailable in the published literature. Furthermore, in light of the foregoing discussion, there is no clear basis for inferring information for two-row systems from available results for one-row systems. The present research was undertaken to provide quantitative results for both the local and average transfer coefficients in a two-row plate fin and tube heat exchanger configuration. Experiments were performed by employing the naphthalene sublimation technique. The mass-transfer results obtained therefrom can be converted to heat-transfer results by means of the heat-mass transfer analogy.

A schematic diagram of the heat exchanger configuration to be studied is shown in Fig. 1. The upper diagram is a pictorial view of a two-row coil in which the tubes are arranged in a staggered array on equilateral triangular centers. The lower diagram is a plan view. Examination of this diagram suggests that there are zones of spanwise symmetry, so that it is sufficient to confine the local transfer coefficient measurements to a typical element bounded by the pair of short-dashed lines. The diagrams also contain dimensional nomenclature as well as the x, y coordinates that will be used to identify positions on the fin surfaces. The portion of the fin contained between $x = 0$ and $x = L$ will be designated as region I, whereas the portion of the fin between $x = L$ and $x = 2L$ will be referred to as region II. These designations will be useful when comparisons are made between the transfer capabilities of the portions of the fin respectively associated with the first and the second rows.

The fin-tube configuration studied here is characterized by the dimension ratios $h/D = 0{\cdot}193$, $S/D = 2{\cdot}5$, and $L/D = 2{\cdot}16$. As discussed in [2], the use of dimension ratios, rather than the actual dimensions,* is a preferable parameterization of the system. The results presented here should be applicable to heat exchangers having dimension ratios in the same range as those mentioned above.

The Reynolds number of the flow was the independent parameter that was varied during the course of the research. The Schmidt number, which is the mass-transfer analogue of the Prandtl number, is 2·5 for the naphthalene–air transfer system. The scaling of the results to correspond to a Prandtl number of 0·7 (heat transfer to air) will be discussed later.

The local and average transfer coefficients will be presented in dimensionless form in terms of the Sherwood number, which plays the same role for mass transfer that the Nusselt number plays for heat transfer. Particular consideration will be given to the relative transfer capabilities of various portions of the fin. To provide unambiguous results for the relative transfer capabilities, dimensionless mass-transfer rates are also presented.

EXPERIMENTS AND DATA REDUCTION

Only a brief description of the experimental apparatus and the data reduction procedure will be given here. Full details are available in [3]. Also, [2] may be consulted for further information on aspects that are common to that investigation and to the present work.

For the mass-transfer experiments, the heat exchanger fins were simulated by specially cast plates of naphthalene. A pair of such plates, together with an array of disks which served both to model the tubes and as separators between the plates, constituted the test section. The number and arrangement of the tubes in the first and second rows is indicated in the lower diagram of Fig. 1.

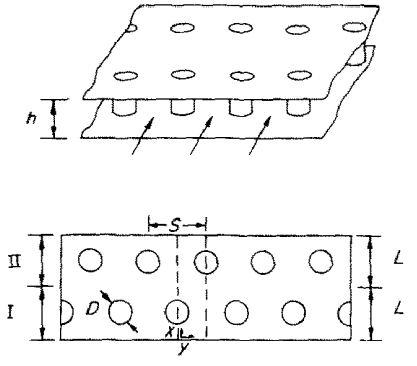

FIG. 1. Schematic of two-row fin and tube heat exchanger configuration.

During a data run, air drawn from the laboratory room was passed through the channel formed between the naphthalene plates. Upon leaving the test section, the air passed successively through a plenum, a calibrated rotameter for flow measurement, a gas meter for corroborating flow measurement, the blower, and then to an exhaust system which vented to the roof of the building. The exhaust system ensured that the laboratory room air was free of naphthalene vapor. The room itself was temperature controlled.

The naphthalene plates were cast in a mold whose metallic components had been hand polished and lapped to a high degree of smoothness and flatness. Removal of the cast plates was accomplished without the aid of lubricants, and the surface quality was such that no subsequent machining was required.

The circular disks used to simulate the heat exchanger tubes were fabricated from delrin, which is a

*The actual values of the apparatus dimensions are: $h = 0{\cdot}165$ cm (0·065 in), $D = 0{\cdot}853$ cm (0·336 in), $S = 2{\cdot}13$ cm (0·840 in), and $L = 1{\cdot}85$ cm (0·727 in).

free-machining plastic. Although the delrin disks faithfully model the hydrodynamics of the tubes in a fin and tube heat exchanger, they do not participate in the mass-transfer process. This is not thought to be a significant factor since the lateral surface area of the disks is only about six per cent of the fin surface area.

Two types of mass-transfer measurements were performed—local and overall. For the local transfer, painstaking measurements of the surface contour of the naphthalene plates were made before and after a data run using a sensitive dial gage whose minimum scale division was 0·00005 in (~0·001 mm). The dial gage was employed in conjunction with a coordinate table which could be traversed to provide for highly accurate settings of the x, y coordinates. In view of the spanwise symmetry that was mentioned earlier, the dial gage measurements were confined to the typical element bounded by the dashed lines in the lower diagram of Fig. 1. The overall mass transfer measurements were accomplished by weighing the naphthalene plates with a precision balance, both before and after a data run.

Owing to the highly complex pattern of surface mass transfer, especially in the second row, contour measurements had to be made at a very large number of points. For instance, at a Reynolds number of 1089, about 1000 discrete surface locations were involved.

The local differences between the surface elevation before and after a data run were carefully corrected for three effects: (a) natural convection sublimation during the time period when the contour measurements were being made; (b) natural convection sublimation during the set-up time of the experiment; (c) elevation changes inherent in removing and subsequent repositioning of the naphthalene plate on the coordinate table. The procedures for making the corrections are outlined briefly in [2] and are described in detail in [3]. The accuracy of the corrections is supported by the excellent closure of the overall mass balances as cited in these references.

From the measured changes in surface elevation, local rates of mass transfer per unit area $\dot{m}(x, y)$ were determined. The spanwise-integrated mass-transfer rate $\dot{M}'$ at any axial station was then obtained by integrating the $\dot{m}$ values in accordance with

$$\dot{M}'(x) = 2\int_{y=0}^{S/2} \dot{m}(x, y)\,\mathrm{d}y \tag{1}$$

in which the factor of 2 accounts for mass transfer at both of the fin surfaces which bound the flow passage. The integrand $\dot{m}(x, y)$ was set equal to zero at fin locations x, y that are blocked out by the tube. Next, the surface-integrated mass-transfer rate (from both bounding fins) for the portion of the fin between $x = 0$ and $x = x$ was found by integration of the $\dot{M}'$ values from equation (1)

$$\dot{M}(x) = \int_{x=0}^{x} \dot{M}'(x)\,\mathrm{d}x. \tag{2}$$

The mass transfer is driven by differences in the concentration of naphthalene vapor. The concentrations that are needed for the evaluation of the transfer coefficients are the bulk and wall values. The bulk concentration of naphthalene vapor at any axial station x, $\rho_{n,bx}$, can be derived from a mass balance, which gives

$$\rho_{n,bx} = \rho_{n,bo} + \dot{M}(x)/\dot{Q} \tag{3}$$

where $\dot{M}(x)$ is from equation (2) and $\dot{Q}$ is the rate of volume flow passing through the typical section bounded by the dashed lines in the lower diagram of Fig. 1. The quantity $\rho_{n,bo}$ is the concentration of naphthalene vapor in the flow entering the test section. In the present experiments, $\rho_{n,bo}$ is zero.

The naphthalene vapor concentration at the plate surface is denoted by $\rho_{n,w}$ and was evaluated from a vapor pressure–temperature relation [4] in conjunction with the perfect gas law. The surface temperature is spatially uniform, so that $\rho_{n,w}$ is also spatially uniform.

The local transfer results will be expressed in terms of a local mass-transfer coefficient K and its dimensionless counterpart, the local Sherwood number, whose definitions are

$$K = \frac{\dot{m}}{\rho_{n,w} - \rho_{n,bx}}, \qquad Sh = \frac{KD_h}{\mathscr{D}}. \tag{4}$$

In the Sherwood number, the quantity $\mathscr{D}$ represents the coefficient of mass diffusion, which is related to the Schmidt number Sc via the definition $Sc = \nu/\mathscr{D}$. The Schmidt number for naphthalene diffusing in air is 2·5.

The hydraulic diameter D_h that appears in the Sherwood number was evaluated in accordance with that defined in the Kays and London treatise on compact heat exchangers [5].

$$D_h = \frac{4\,(\text{minimum flow area})\,(\text{streamwise length})}{\text{transfer surface area}}. \tag{5}$$

To facilitate the application of the present results to heat-transfer situations, the lateral area of the tubes was included in the denominator of equation (5).

Average transfer coefficients were evaluated for the two-row coil as a whole. Let $\dot{M}_{\text{total}}$ be the overall rate of mass transfer, A_{total} the corresponding fin surface area, and $(\Delta\rho_n)_m$ the log-mean concentration difference. With these, one can define

$$\overline{K} = \frac{(\dot{M}/A)_{\text{total}}}{(\Delta\rho_n)_m}, \qquad \overline{Sh} = \frac{\overline{K}D_h}{\mathscr{D}}. \tag{6}$$

The log-mean concentration difference that appears in equation (6) is expressed by

$$(\Delta\rho_n)_m = \frac{(\rho_{n,w} - \rho_{n,bo}) - (\rho_{n,w} - \rho_{n,b2L})}{\ln[(\rho_{n,w} - \rho_{n,bo})/(\rho_{n,w} - \rho_{n,b2L})]}. \tag{7}$$

The quantity $\rho_{n,b2L}$ is the bulk concentration at exit ($x = 2L$). It was evaluated from equation (3) with $\dot{M}(x)$ replaced by $\dot{M}_{\text{total}}$.

To aid in assessing the transfer capabilities of different parts of the fin, overall rates of mass transfer have also been determined for the portions of the fin respectively associated with the first and second rows of tubes. These portions of the fin are designated as I and II in the lower diagram of Fig. 1. For each region, the

respective overall transfer rates were taken from equation (2), with

$$\dot{M}_{\mathrm{I}} = \dot{M}(L), \quad \dot{M}_{\mathrm{II}} = \dot{M}(2L) - \dot{M}(L). \tag{8}$$

These results will be presented in ratio form as $\dot{M}_{\mathrm{I}}/\dot{M}_{\mathrm{total}}$ and $\dot{M}_{\mathrm{II}}/\dot{M}_{\mathrm{total}}$.

The Reynolds number employed to parameterize the results is that of Kays and London [5].

$$Re = D_h G/\mu \tag{9}$$

in which D_h is the hydraulic diameter of equation (5) and G is the mass velocity at the minimum flow cross section. Other Reynolds numbers are sometimes used for flow passages such as those of this research. The relationship of various other Reynolds numbers to that employed here is listed in Table 1 of [2].

RESULTS AND DISCUSSION

The mass transfer results to be presented here may be converted to heat-transfer results by employing the heat-mass transfer analogy. As noted earlier, the boundary condition for the mass-transfer experiments was uniform wall concentration of the naphthalene vapor which corresponds, by analogy, to uniform wall temperature for the heat-transfer case. Thus, the present results can be used for heat-transfer applications when a correction is made for values of fin efficiency that are less than one.

According to the analogy, which is more fully discussed in [2], the conversion between the Sherwood and Nusselt number results can be accomplished by the relations

$$Nu = (Pr/Sc)^n Sh, \quad \overline{Nu} = (Pr/Sc)^m \overline{Sh} \tag{10}$$

where n and m are usually 1/3 or 0·4.

Local results

Attention will now be turned to the transfer mechanisms which are operative in the two-row fin and tube exchanger, and for this purpose the surface distributions of the local transfer coefficients will be presented and discussed. Owing to the complexity of the results, such a presentation is very space consuming and will, therefore, be limited to two Reynolds numbers, $Re = 1089$ and 211. Information for a third Reynolds number, $Re = 649$, is available in [3].

The distributions of local Sherwood number for $Re = 1089$ are presented in Figs. 2(a–c). These figures are made up of a succession of graphs, with each graph portraying the spanwise distribution of the local Sherwood number at a given axial station characterized by x/L. The graphs for the smallest x/L positions are at the lower left of Fig. 2(a) and the successive graphs proceed downstream to larger x/L. Figure 2(a) terminates with $x/L \cong 1$, and Fig. 2(b) follows on with x/L values up to about 1·3. Graphs for axial stations between x/L of 1·3 and 2 are contained in Fig. 2(c). Each of the graphs has its own ordinate scale to accommodate the range of Sherwood numbers at that axial station.

Axial stations characterized by $x/L < 0{\cdot}269$ lie upstream of the first row, those with x/L between 0·731 and 1·269 lie between the first and second rows, and those with $x/L > 1{\cdot}731$ lie downstream of the second row.

Examination of Fig. 2(a), which corresponds to the portion of the fin associated with the first row of tubes, reveals the presence of transfer mechanisms already noted in the Introduction. The developing boundary layers in the forward part of the channel yield relatively high transfer coefficients which decrease in the flow direction. The blockage of the channel by the tube has an upstream influence and causes a spanwise variation of the transfer coefficients.

In front of the tube, high peaks in the distribution curves are in evidence. These peaks constitute a natural augmentation caused by a vortex system which develops in front of the tube and is swept around the side. For the Reynolds number of Fig. 2, there are two peaks, a primary one and a much lesser one. The transfer coefficients at the primary peak are substantially higher than are those in the boundary-layer region. The peaks persist around the side of the tube and, at this Reynolds number, disappear at $x/L \sim 0{\cdot}7$. The region downstream of the tube is one of generally low transfer coefficients, with remarkably low values in the wake.

Figure 2(b) contains results for the initial part of the fin surface that is associated with the second row of tubes. The axial stations portrayed therein lie between $x/L = 1$ and 1·29 (note that the forward edges of second-row tubes are at $x/L = 1{\cdot}269$). As can be seen from the figure, the regime of generally low transfer coefficients (including the depressed wake region) that was inherited from the first row is perpetuated in the initial portion of the second-row fin. Then, owing to a vortex system which develops in front of the second row of tubes, peaks begin to appear in the transfer coefficient distributions.

With respect to these peaks, it is relevant to note that, owing to the channelling caused by the first row of tubes, the velocity of the flow approaching the second row is substantially higher than that approaching the first row. Furthermore, it has been found [2] that the height of the peaks, the number of peaks in a distribution curve, and the downstream persistence of the peaks is accentuated with increasing approach velocity. It would, therefore, be expected that the vortex system spawned by the second row of tubes would play a relatively more important role than that played by the vortex system of the first row.

This expectation is verified by comparing the distribution curves of Fig. 2(b) with those in Fig. 2(a) for the region just upstream of the first row. The local Sherwood numbers attained by the peaks of the second row are seen to be about 50 per cent higher than those of the first row. In fact, even the secondary peaks in the second-row distribution curves are substantially higher than the primary peaks in the first-row distribution curves. A small tertiary peak is also in evidence in the distributions of Fig. 2(b). Another interesting observation in Fig. 2(b) is that the region

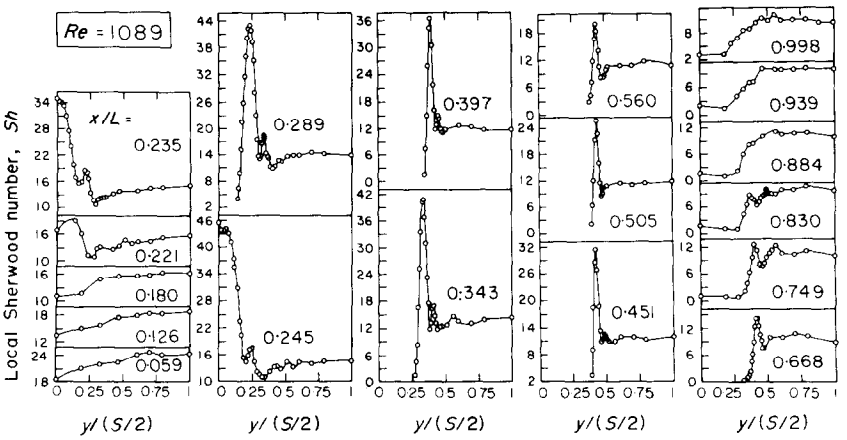

FIG. 2(a). Distributions of local Sherwood number on the fin surface, $Re = 1089$ and $Sc = 2{\cdot}5$.

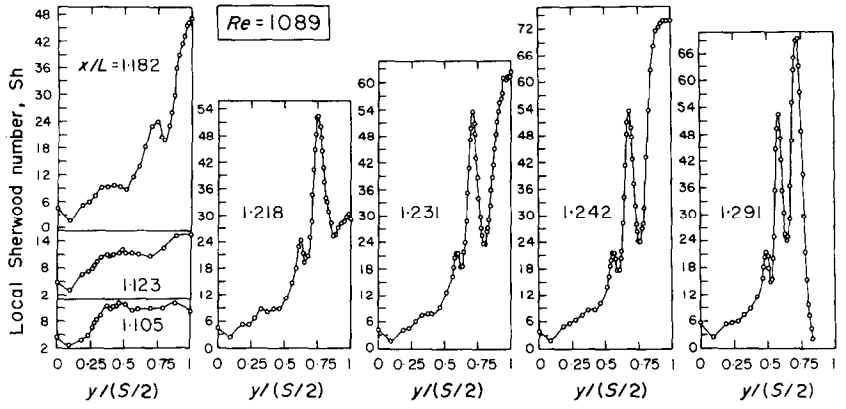

FIG. 2(b). Distributions of local Sherwood number on the fin surface, $Re = 1089$ and $Sc = 2{\cdot}5$.

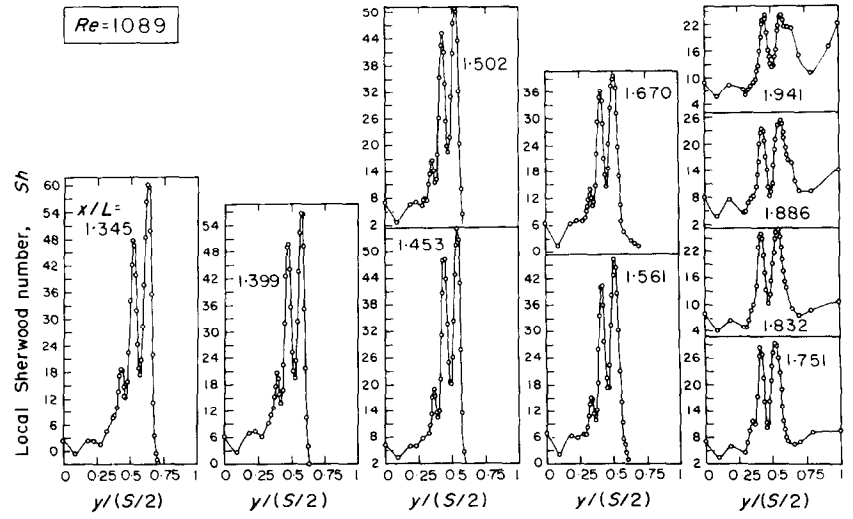

FIG. 2(c). Distributions of local Sherwood number on the fin surface, $Re = 1089$ and $Sc = 2{\cdot}5$.

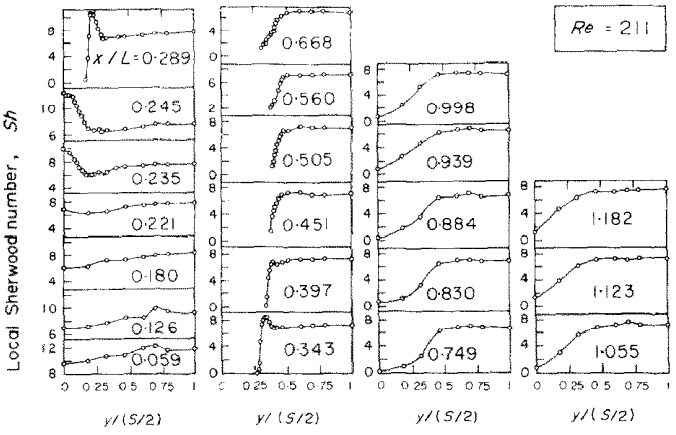

FIG. 3(a). Distributions of local Sherwood number on the fin surface, $Re = 211$ and $Sc = 2{\cdot}5$.

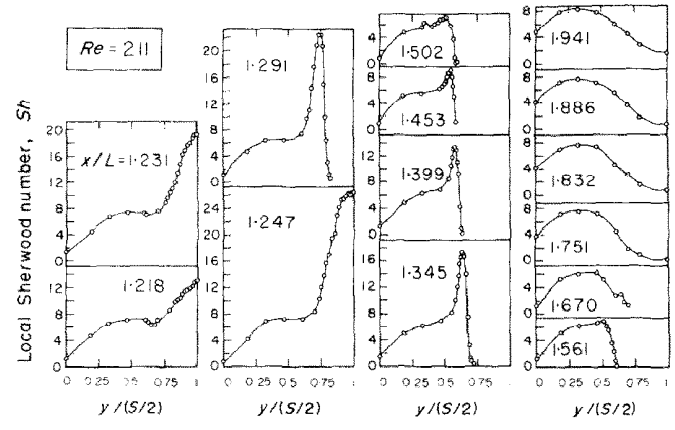

FIG. 3(b). Distributions of local Sherwood number on the fin surface, $Re = 211$ and $Sc = 2{\cdot}5$.

of very low transfer coefficients resulting from the wake of the first row continues to be present in all of the distribution curves.

The spanwise distributions at the side and downstream of the second-row tubes are presented in Fig. 2(c). The figure shows that all three peaks in the distribution curves persist, although with somewhat decreasing magnitude, to the downstream end of the tube ($x/L = 1{\cdot}73$). The distribution curves do not extend all the way to $y/(S/2) = 1$ owing to the presence of the tubes. The influence of the wake region of the first row continues to be in evidence.

Just downstream of the tubes (i.e. at $x/L = 1{\cdot}751$), the distribution curve consists of a pair of peaks flanked on either side by lower plateaus which are related to the wakes shed by the first and second rows. It is interesting to note that the transfer coefficients in the wake of the second row are substantially higher than are those in the wake of the first row. As one proceeds to larger x/L, the coefficients in the wake of the second row tend to "fill in", while the peaks diminish slightly in magnitude and tend to broaden.

It is clear that there are major differences in the transfer coefficient distributions for the portions of the fin respectively associated with the first and second rows. These differences are related to differences in the relative importance of various transfer mechanisms. The Reynolds number of the flow also has a first-order influence on the shapes of the distribution curves and on the relative importance of the various transfer mechanisms. Figures 3(a) and (b), which correspond to $Re = 211$, have been prepared to illustrate this point.

Examination of Fig. 3(a) gives an immediate indication that the first-row vortex system and the corresponding peak in the distribution curves are substantially weaker than at higher Reynolds numbers. Not only are the peaks of relatively lesser magnitude, but they are also quickly dissipated and are, therefore, in evidence at only a few axial stations. From Fig. 3(b), it is seen that the vortex system associated with the second row of tubes is stronger than that associated with the first row, as was also the case at the higher Reynolds number. However, there is only a single peak, and it persists only to an axial station about half way around the tube (i.e. up to $x/L \sim 1{\cdot}5$), whereafter it disappears. Downstream of the second row, the wake which is shed from the second row of tubes causes low values of the transfer coefficients, whereas the wake carried back from the first row of tubes tends to "fill in". As expected, the overall level of the Sherwood numbers of Fig. 3 is substantially lower than the level of those of Fig. 2.

Integrated and average results

The relative transfer capabilities of various portions of the fin will now be examined from another viewpoint. In the prior section of the paper, the spanwise-integrated mass-transfer rate $\dot{M}'(x)$ at any axial station x was introduced via equation (1). The variation of $\dot{M}'$ with x gives an indication of which axial stations transfer greater amounts of mass and which stations transfer lesser amounts. To achieve a dimensionless presentation, we form the ratio

$$\frac{\text{mass-transfer rate at axial station } x}{\text{average of the transfer rates at all axial stations}}. \quad (11)$$

The numerator is $\dot{M}'(x)$, while the denominator is evaluated from

$$\frac{1}{2L}\int_{x=0}^{2L} \dot{M}'(x)\,dx. \quad (12)$$

where the full fin area is restored, the spanwise-integrated values are low because the local mass-transfer rates are low.

A final inspection of Fig. 4 affirms the different patterns of mass transfer on the portions of the fin respectively associated with the first and second rows. For the former, the greatest contribution to the mass transfer is from the boundary-layer region, with an assist from the vortex region in front of the tubes. On the other hand, for the latter, the vortex region provides the largest contribution.

A note of caution should be sounded about comparing the results of Fig. 4 for the range $0 \leqslant x/L \leqslant 1$ with those for one-row coils that are presented in Fig. 6 of [2]. The denominator of the ordinate variable of Fig. 4 is an average over both rows of a two-row coil. On the other hand, the denominator of the ordinate variable of Fig. 6 of [2] is an average over a one-row

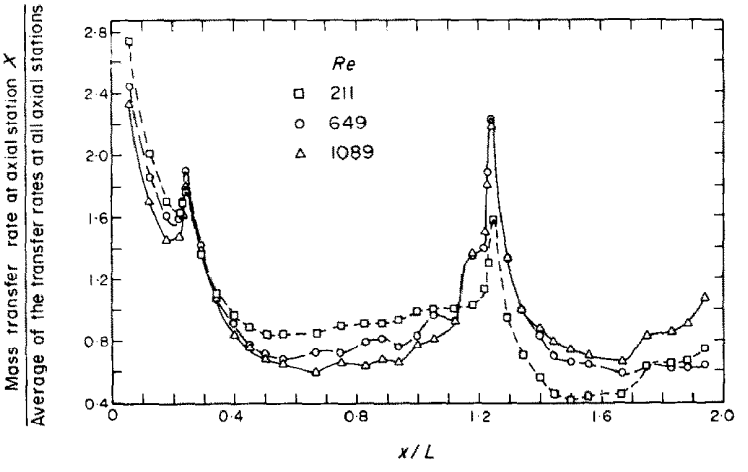

FIG. 4. Variation of the spanwise-integrated mass-transfer rate.

The variation of the spanwise-integrated mass transfer as a function of axial position is presented in Fig. 4 for three Reynolds numbers, $Re = 211$, 649 and 1089. Owing to the dimensionless nature of the ordinate variable, the areas under all three of the curves are the same and equal to two. From the figure, it is seen that the regions of high mass transfer are the boundary-layer development zone at the forward part of the fin and the vortex-dominated zones adjacent to the upstream faces of the first and second rows of tubes. The mass-transfer rates in the vortex zones, especially that of the second row, are particularly impressive at the higher Reynolds numbers. At low Reynolds numbers, the transfer rates in the vortex zones are substantially less than those in the boundary-layer zone.

The regions of relatively low mass transfer are seen to be at the sides of the tubes and downstream of the tubes. The low values in evidence at the axial stations situated at the sides of the tubes ($0{\cdot}269 < x/L < 0{\cdot}731$ and $1{\cdot}269 < x/L < 1{\cdot}731$) are due, in part, to the reduced fin surface area due to the presence of the tubes (note that the ordinate is the spanwise-integrated mass transfer). At axial stations downstream of the tubes, coil. This difference between the denominators precludes a meaningful comparison between the figures.

Further information about the relative transfer capabilities of the two portions of the fin is given in Table 1. The quantities $\dot{M}_{\mathrm{I}}$ and $\dot{M}_{\mathrm{II}}$, which are defined in equation (8), respectively denote the overall rates of mass transfer in regions I and II. These regions are illustrated in the lower diagram of Fig. 1 and correspond to the portions of the fin associated with the first and second rows.

From the table, it is seen that the lower the Reynolds number, the greater is region I's share of the total mass transferred by the system. For instance, at $Re = 211$, almost two-thirds of the mass transfer takes place in

Table 1. Relative transfer capabilities of Regions I and II

Re	$\dot{M}_{\mathrm{I}}/\dot{M}_{\mathrm{total}}$	$\dot{M}_{\mathrm{II}}/\dot{M}_{\mathrm{total}}$
211	0·635	0·365
649	0·572	0·428
1089	0·526	0·474

region I. As the Reynolds number increases, more and more of a parity is established between the two regions, so that for $Re = 1089$, region I's share is 52·6 per cent. These results affirm the growing importance of the vortex systems as the Reynolds number increases and, in particular, of the vortex system adjacent to the second row of tubes.

The transfer capabilities of the two-row coil as a whole will be presented in terms of the average Sherwood number, which is the dimensionless counterpart of the average mass-transfer coefficient. These quantities are defined in equations (6) and (7). Results for the average Sherwood number are plotted in Fig. 5 as a function of the Reynolds number over the range from $Re = 160$ to $Re = 1270$. A curve has been faired through the data points (black circles) to provide continuity.

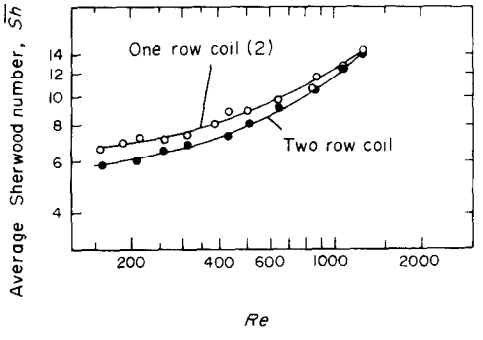

FIG. 5. Average Sherwood numbers as a function of Reynolds number, $Sc = 2{\cdot}5$.

The Sherwood number is seen to increase with the Reynolds number, as is intuitively reasonable. Furthermore, the fact that the $\overline{Sh}$ vs Re relationship is not a straight line is also reasonable. In view of the growing contributions of the vortex systems with increasing Reynolds numbers, the more rapid rise of $\overline{Sh}$ with Re at the larger Reynolds numbers, as indicated in the figure, is as it should be.

For comparison, average Sherwood number results are plotted in Fig. 5 for a one-row coil having the same dimension ratios as the present two-row coil. The data for the one-row coil are from [2]. At the lower Reynolds numbers, the Sherwood numbers for the one-row coil are 10–15 per cent higher than those for the two-row coil. The gap between the two sets of results closes at the higher Reynolds numbers. This behavior is readily understood in terms of the results presented and discussed in connection with Table 1. There, it was found that at low Reynolds numbers, the second-row fin of a two-row coil was less effective as a transfer surface than the first-row fin. This is because the first row has a major boundary-layer contribution, whereas the second row has no boundary-layer contribution and only a modest vortex contribution. At higher Reynolds numbers, the vortex contribution brings the second-row fin to a point of near equality relative to the first-row fin.

The overall mass-transfer rates obtained by integration of the local values [via equation (2)] were compared with those determined by direct weighing of the naphthalene plates. For the three data runs where the comparisons were made, the agreement was within 3·5–4 per cent. In view of the complex local mass-transfer distributions that had to be integrated, this level of agreement is believed to be highly satisfactory.

CONCLUDING REMARKS

The results of this investigation have established both the qualitative and quantitative characteristics of the transfer capabilities of two-row plate fin and tube heat exchangers. Different transfer mechanisms were found to be operative on the portions of the fin which are respectively associated with the first and second rows of tubes. For the first-row fin, the boundary-layer development is, perhaps, the most important factor, with the vortex-induced transfer gaining in importance at higher Reynolds numbers. On the other hand, for the second-row fin, there is no region of boundary-layer development, and it is the vortex system alone which is responsible for regions of high transfer. The influence of the second-row vortex system is accentuated at higher Reynolds numbers.

The vortex systems represent a natural augmentation mechanism, as does the boundary-layer development. If artificial augmentation devices are considered, it would appear necessary to examine their impact on the already existing natural augmentation.

The results of the present investigation, as well as those of [2], cast a shadow of uncertainty on the conventional method of evaluating the efficiency of the fins in a plate fin and tube heat exchanger. The normal procedure is to assume that the heat-transfer coefficient is uniform at all points on the fin surface and to employ results based on one-dimensional radial heat conduction in an annular fin. The local results presented herein and in [2] indicate that there are large spatial variations in the transfer coefficients. Such variations, when impressed on a fin, would give rise to two-dimensional heat conduction within the fin. There is, clearly, a need to examine the importance of these influences on fin design.

Acknowledgement—Scholarship support extended to F. E. M. Saboya by the Conselho Nacional de Pesquisas and by the Instituto Tecnologico de Aeronautica (both Brazilian institutions) is gratefully appreciated.

REFERENCES

1. D. R. Rich, The effect of fin spacing on the heat transfer and friction performance of multi-row, smooth plate fin and tube heat exchangers, ASHRAE preprint 2288 (1973).
2. F. E. M. Saboya and E. M. Sparrow, Local and average transfer coefficients for one-row plate fin and tube heat exchanger configurations, *J. Heat Transfer* **96**, 265–272 (1974).
3. F. E. M. Saboya, Local and average transfer coefficients in a plate fin and tube exchanger configuration, Ph.D. Thesis, Department of Mechanical Engineering, University of Minnesota, Minneapolis, Minnesota (1974).
4. H. H. Sogin, Sublimation from disks to air streams flowing normal to their surfaces, *Trans. Am. Soc. Mech. Engrs* **80**, 61–71 (1958).
5. W. M. Kays and A. L. London, *Compact Heat Exchangers*, 2nd edn. McGraw-Hill, New York (1964).

CARACTERISTIQUES DE TRANSFERT DES ECHANGEURS DE CHALEUR A DEUX RANGEES DE TUBES AVEC AILETTES PLANES

Résumé—L'analogie entre transferts de chaleur et de masse a été utilisée, en conjonction avec une technique de sublimation du naphtalène afin d'étudier les performances et les mécanismes de transfert dans les échangeurs de chaleur à deux rangées de tubes avec ailettes planes. Les coefficients de transfert locaux et moyens ont été déterminés à partir de mesures de la masse transportée dans un système analogique composé de deux plaques de naphtalène et d'une rangée de disques d'espacement. Le système analogique était construit sur le modèle d'une section de passage d'un échangeur de chaleur type. Les résultats ont été présentés sous forme adimensionnelle afin de faciliter leur transposition en nombres de Nusselt.

Des mécanismes de transfert différents ont été constatés agir sur les portions de l'ailette respectivement associées à la première et à la seconde rangée de tubes. Sur la portion associée à la première rangée, les deux facteurs qui ont fourni des taux de transfert de masse élevés sont la couche limite à l'avant de l'ailette et le système tourbillonnaire qui se développe devant les tubes. D'autre part, sur la portion de l'ailette associée à la deuxième rangée, il n'y a pas de régime de couche limite, et c'est le système tourbillonnaire seul qui est responsable des taux de transfert élevés. A des nombres de Reynolds plus grands, l'influence du système tourbillonnaire associé à la deuxième rangée est suffisante pour assurer une égalité approchée des possibilités de transfert des surfaces de l'ailette associées à la première et à la seconde rangée.

ÜBERTRAGUNGSVERHALTEN VON ZWEIREIHIGEN RIPPENROHRWÄRMEÜBERTRAGER-ANORDNUNGEN

Zusammenfassung—Die Wärme-Stoffübertragungs-Analogie aufgrund der Naphthalin-Sublimations-Technik wurde verwendet um die Übertragungsmöglichkeiten und Übertragungsmechanismen in zweireihigen Rippenrohrwärmeübertrager-Anordnungen zu untersuchen. Örtliche und mittlere Übergangskoeffizienten wurden aus dem Stoffübergang bestimmt in einem Analogiesystem, das aus einem Paar Napthalin-Platten und einer Anordnung von Abstandscheiben bestand. Das Analogiesystem sollte das Modell eines typischen Wärmeübertrager-Strömungskanals darstellen. Die Ergebnisse wurden in dimensionsloser Form angegeben, um ihre Übertragbarkeit in Nusselt–Zahlen zu erleichtern.

Unterschiedliche Übertragungsmechanismen ergaben sich für die Rippen der ersten und zweiten Reihe der Rohre. Für die erste Reihe ergaben sich zwei Faktoren für hohen Stoffübergang: die Grenzschicht an der strömungszugewandten Seite der Rippe und ein Wirbelsystem, das sich vor den Rohren aufbaut. Für die zweite Reihe ist kein Grenzschichtregime vorhanden und das Wirbelsystem allein ist für die hohen Übertragungsleistungen verantwortlich. Bei höheren Reynolds–Zahlen reicht der Einfluß des Wirbelsystems der zweiten Rohrreihe aus, um Gleichheit im Übergang von den Rippenflächen der ersten und zweiten Reihe zu erreichen.

ХАРАКТЕРИСТИКИ ПЕРЕНОСА ДВУХРЯДНЫХ ПЛАСТИНЧАТО-РЕБЕРНЫХ И ТРУБЧАТЫХ КОНФИГУРАЦИЙ ТЕПЛООБМЕННИКОВ

Аннотация — Для исследования характеристик и механизмов переноса двухрядных пластинчато-реберных трубчатых конфигураций теплообменников использовалась аналогия тепло- и массообмена вместе с техникой сублимации нафталина. Локальные и средние коэффициенты переноса определялись по данным измерения массы, переносимой в аналогичной системе, состоящей из двух нафталиновых пластин и ряда распорных дисков. В аналогичной системе моделировалось течение в типичном теплообменнике. Результаты представлялись в безразмерном виде для облегчения их перевода в числа Нуссельта.

Найдено, что на отрезках ребра, связанных с первым и вторым рядами труб, действуют различные механизмы переноса. На отрезке ребра, связанном с первым рядом, высокие скорости переноса массы имеют место благодаря пограничному слою на передней части ребра и вихреобразованию, развивающемуся перед трубами. С другой стороны, на отрезке ребра, связанного со вторым рядом, режим пограничного слоя отсутствует, и только вихреобразование вызывает высокие скорости переноса. При больших значениях числа Рейнольдса влияния вихревой системы второго ряда достаточно для того, чтобы характеристики переноса поверхностей ребер первого и второго рядов были почти одинаковыми.